The Integrated Voxel Analysis Method to Diagnose Onset of Alzheimer's Disease and Pinpoint Severely Affected Brain Regions through Structural MRI Images

Armen Aghajanyan
Cell Phone: (425) 922-5420:
armen.ag@live.com

Matthew Hur
Cell Phone (425) 495-6845:
hurmatthew@gmail.com

***Abstract*—Magnetic Resonance Imaging (MRI) provides three-dimensional anatomical and physiological details of the human brain. We describe the Integrated Voxel Analysis Method (IVAM) which, through machine learning, classifies MRI images of brains afflicted with early Alzheimer's Disease (AD). This fully automatic method uses an extra trees regressor model in which the feature vector input contains the intensities of voxels belonging to corresponding regions in the brain, whereby the effect of Alzheimer's on a single voxel can be predicted. The resulting tree is used in the following two steps: a K-nearest neighbor (KNN) algorithm based on Euclidean distance with the feature vector to classify whole images based on their distribution of affected voxels and a voxel-by-voxel classification by the tree of every voxel in the image. Voxel-by-voxel classification is followed by an Ising model filter to remove artifacts and to facilitate clustering of the classification results which identifies significant voxel clusters affected by AD. We apply this method to T1-weighted MRI images obtained from the Open Access Series of Imaging Studies (OASIS) using images belonging to normal and early AD-afflicted individuals associated with a Client Dementia Rating (CDR) which we use as the target in the supervised learning. Furthermore, statistical analysis of the results is conducted using pre-labeled brain atlases to automatically pinpoint significantly affected brain regions. While achieving 96% AD classification accuracy on 233 images in the OASIS dataset, the method reveals morphological differences caused by the onset of AD.**

***Keywords*—Biomedical image processing,Medical diagnostic imaging,Predictive models,Machine learning,Decision trees**

I. Introduction

Alzheimer's Disease (AD) is a prevalent degenerative disorder in today's society as the 7th leading cause of death in America (Speert et al., 2012). As the causes and inner mechanisms underlying AD-related brain abnormalities are not fully understood, no cure has yet been found; however, treatments such as pharmacology that inhibit acetylcholinerase have successfully prolonged the lifespan of affected individuals by slowing down the degeneration of acetylcholine-releasing neurons (Bianchetti et al., 2006). Other biomolecular phenomena including the formation of beta-amyloid plaques and tao-fibrillary tangles have been implicated, but its relation to macroscopic mechanisms concerning brain regions is still nebulous. Current initial diagnosis is made clinically with final confirmation made through direct examination of brain tissue. Computational methods for classification and segmentation can facilitate and supplement clinical diagnosis.

In order to reveal these macroscopic mechanisms between brain regions, many current image classification and segmentation algorithms incorporate an essential step of feature extraction. For example, the widely used and effective Voxel-Based Morphometry (VBM) method is designed for feature extraction to determine specific anatomic patterns of cerebral atrophy (Ashburner and Friston, 2000). However, this method suffers from its dependence on an precise registration and warping of MRI images to *a priori* probability maps (Veress et al., 2013). Its high sensitivity to accurate registration creates a limitation because the templates inherently differ with various MRI images due to structural variance of brain shape. Additionally, its high computational complexity leads to difficult implementation and long run-time. Other methods for segmentation such as the Hybrid Watershed Algorithm (HWA) and the Brain Extraction Methods (BEM and BEM2DE) rely on accurate iterative thresholding and also rely on assumptions about brain shape that limit their practical use when analyzing variegated brain shapes belonging to subjects of various demographic groups (Fennema-Notestine et al., 2006). Fully automatic methods need to quickly and effectively account for individual differences in brain shape without human supervision.

The essential steps that improve the results in these automatic methods are energy-based deformation fields which identify regions of interest, whereby a driving force pushes an objective function to convergence. Success of the energy methods can be attributed to the utilization of information about local differences as well as about global trends of the image.

We propose a multifaceted algorithm that utilizes white-box methods for decision-tree learning to robustly and automatically classify AD affected brains as well as cluster and segment classification results of individual voxels to yield severely affected brain regions. At the center of our framework of integrated processes is a trained extra trees regressor known to be highly effective for supervised learning of complex data (Geurts et al., 2006). The trained model is used then to estimate the distribution of Alzheimer affected voxels, which are sampled from the MRI. A second model is placed on top of the distributions to predict the CDR of the whole brain. The

aggregated learning model can also relay information about specific affected brain regions allowing for novel insights into the inner neurological workings of AD tailored to accurately diagnose AD in its early stages.

II. Data and Preprocessing

A. Data Set

We obtain 233 anonymous MRI images from the Open Access Series of Imaging Studies (OASIS) (Buckner et al., 2004). Their age range is from 18-96 years with a mean of 53 years with each clinically diagnosed with a Client Dementia Rating (CDR) which rates subjects based on 6 criteria: memory, orientation, judgment and problem solving, function in the community, home and hobbies, and personal care (Buckner et al., 2004). The values range from 0 to 3 where 0 indicates no dementia while 0.5 and 1 indicate very mild and mild dementia respectively. In order to specifically analyze the onset of AD and due to the sparsity of the dataset of images labeled with a CDR > 1, we use images labeled with a CDR of 0, 0.5, and 1. All images are T1-weighted prepared rapid echo-gradient and obtained on a 1.5-T vision scanner. (Buckner et al., 2004). Acquisition matrix was [256 256] with 128 contiguous saggital slices of thickness of 1.25 mm.

B. Spatial Normalization

One of the most essential components to accurate analysis of MRI images is the spatial normalization of the dataset. Through co-registration, processing of MRI images can be compared across multiple subjects, especially important for brain Region of Interest (ROI) analysis in pinpointing the affected regions. The images were normalized to the template provided by the Montreal Neuroimaging Institute known as the MNI152 template built by averaging across 152 brains. The images were first converted to the same voxel resolution of 1mm x 1mm x 1mm and symmetrically zero-padded to transform to the same dimensions. Next, each image was registered to the MNI152 template using a one plus one evolutionary optimizer to maximize the mutual information metric provided by David Mattes (Mattes et al., 2001).

III. Voxel by Voxel Regression Model

A. Feature Selection and Building the Supervised Data-set

Our feature selection algorithm was based on the assumption that the level of Alzheimer's projected at a voxel was solely based on the surrounding voxels as well as the three-dimensional coordinate point where our voxel of interest lay. Consequently, our feature vector included the values of all voxels around the voxel of interest with a preset radius and the appended 3D coordinates of the voxels of interest as well as the gender of the subject as male and female brain anatomy have been shown to exhibit strucutral differences.

For each MRI we enumerate all coordinates where the surrounding points are not all zeros. For each voxel we selected features as described above. Because of the sheer size of MRI images, we added a variable step constant throughout the whole aggregated model. Instead of enumerating every point, the step dictates step incrementation in the coordinates for the voxel of interest.

Below is the code for feature selection:

```
def feat(slice,k=10,step=None,add=None):
    shape = slice.shape
    step = step or k
    lenx = shape[0]
    leny = shape[1]
    lenz = shape[2]
    h = k / 2
    lista = []

    for x in range(k,lenx - half,step):
      for y in range(k,leny - half,step):
        for z in range(k,lenz - half,step):
          t = slice[x-h:x+h,y-h:y+h,z-h:z+h]
          data = np.reshape(t,-1)
          if np.all(data == 0):
            continue
          if add:
            data = np.append(data,add)
            data = np.append(data,[x,y,z])
          lista.append(data)
    return lista
```

B. Building the Model

The label of each feature vector is simply the CDR rating of respective patient. Once we built the data-set, we randomly sampled half of the data and used that to train a the ensemble, Extra Random Trees Regressor (Geurts et al., 2006) using the popular sklearn library (Pedregosa et al., 2011). Although it is recommended to use the Extra Random Tree Regressor with an ensemble method such as Random Forests (Geurts et al., 2006), through experimentation we saw that we suffered losses in accuracy when using an ensemble. This model now allows us to predict the CDR rating of a single voxel in the MRI.

IV. Predicting the CDR of the Patient

Our method for predicting the CDR of a patient stems from our axiomatic assumption that the severity of Alzheimer's disease in a patient, will be represented by the distribution of individual CDR regressed voxels. Our first intuition was to use the Kullback-Leibler divergence (Kullback and Leibler, 1951) as a tool to compare the distributions. Although this gave us promising results, the utilization of K-Nearest Neighbor (Bentley, 1975) achieved much greater accuracy than the Kullback-Leibler divergence. Sampling from the brain was done in the same way as the feature selection, using the same function as well. After sampling, the regression model was used to predict the CDR of each individual voxel. The label or target for the KNN algorithm was the CDR of the respective patient. The accuracy will be introduced at the Discussion section below.

V. Pinpointing Severely Affected Brain Regions

The process of pinpointing severely affected brain regions from MRI's can be seen as a pipelining process.

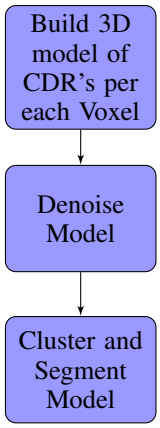

A. Building the 3D Model

Building the 3D Model

```
def target_brain_regions(slice,k,add,model):
  shape = slice.shape

  lenx = shape[0]
  leny = shape[1]
  lenz = shape[2]
  half = k / 2

  lista = np.zeros(shape)

  for x in range(0,lenx - half):
    print(x)
    for y in range(leny - half):
      def inner_loop(z):
        t = slice[x-h:x+h,y-h:y+h,z-h:z+h]
        data = np.reshape(t,-1)
        if np.sum(data) == 0:
          lista[x,y,z] = -2
          return
        if add:
          data = np.append(data,add)
          data = np.append(data,[x,y,z])
        lista[x,y,z] = model(data)

      map(inner_loop,xrange(lenz - half))
  return np.array(lista)
```

The image below is a saggital half-brain slice of a normalized MRI image for comparison to the CDR classified image that follows:

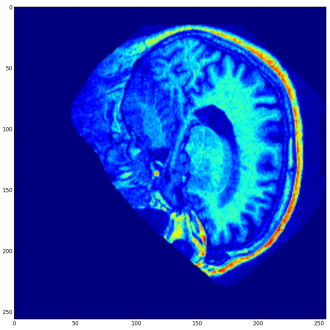

The next image depicts the results of the denoising model applied to the CDR voxel predictions. Black, grey, and white correspond to CDR predictions of 0, 0.5, and 1 respectively.

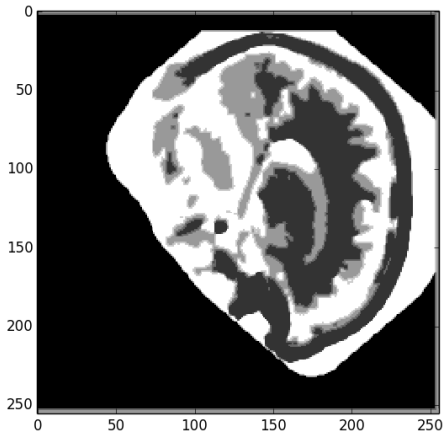

B. Denoising via Ising Model

Using Murphy's (Murphy, 2012) derivation of the Ising model, we define the probability of the update as

$$\log \tilde{p}(y) = -\sum_{s \neq t} y_s w_{st} y_t \tag{1}$$

The weight w_{st} signifies the amount we attribute to the difference between the two pixels. To simplify the calculations, we modify our equation to:

$$\log \tilde{p}(y) = \frac{1}{2} y^T W y \tag{2}$$

where W is a Toeplitz matrix. We define our objective function as

$$argmax_x p(y,x) = p(x)p(y|x) \tag{3}$$

. Continuing, by Murphy's derivation (Murphy, 2012), the unnormalized prior is as follows:

$$p(x) = \frac{1}{Z_0} exp(-E_0(x)) = \frac{1}{Z_0} exp(\sum_i \sum_{j \in nbhd(i)} W_{ij} x_i x_j) \tag{4}$$

. The Z_0 is not needed since we are using the unnormalized prior. On the other hand, our unnormalized posterior will be:

$$p(x|y) = \frac{p(y|x)p(x)}{p(x,y)} = \frac{1}{Z} exp(\sum_i L_i(x_i) - E_0(x)) \tag{5}$$

For the mean field update, we need to compute (see Murphy section 21.3.1 for details)

$$\log q_j(x_j) = E_{-q_j}[\log \tilde{p}(x)] + const \tag{6}$$

and since

$$E_{-q_j}(f) = \sum_{k \neq j} q(x_j, \mu_j | x_j) f(j) = \sum_{k \neq j} q(\mu_j) f(j), \tag{7}$$

we have

$$q_i(x_i) \propto exp(x_i \sum_{j \in nbhd(i)} W_{ij} \mu_j + L_i(x_i)). \tag{8}$$

which yields the important theoretical step. Murphy derives an actual update. In Murphy's (Murphy, 2012) derivation (page 738), note that it uses

$$L_i^+ \equiv L_i(+1) \; and \; L_i^- \equiv L_i(-1) \tag{9}$$

which are the log likelihood functions centered at each of these two values. The variance in the likelihood controls the strength of the prior. This is the final update, which also incorporates a damping term:

$$\mu_i^t = (1-\lambda)\mu_i + \lambda \tanh\left(x_i \sum_{j \in nbhd(i)} W_{ij}\mu_j + 0.5(L_i^+ - L_i^-)\right) \tag{10}$$

To convert this algorithm into a tertiary denoiser we introduced this function to convert CDR to Ising denoiser values.

$$(2 * CDR) - 1 \tag{11}$$

C. Clustering and Segmentation Model

Our clustering and segmentation model was based on Ward's method (Ward, 1963). We input the connectivity matrix of the denoised image into Ward's hierarchical clustering method. The connectivity matrix can be defined as a matrix where each sample is defined through the neighboring samples following a given structure of the data. The structure in our data was simply a graph of the voxel-by-voxel connections. Below is the segmented model.

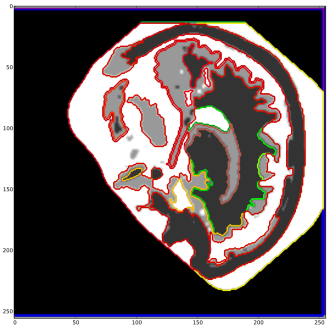

VI. Discussion

In this paper we introduced a novel approach to classifying the dementia rating of a patient from a T1 weighted structural MRI. An extension of our model was the ability to classify and segment parts of the brain that were most affected by AD. Below is a comparison of approaches that tested accuracy on the same OASIS dataset.

Algorithm Type	Accuracy on OASIS Data Set
IVAM Binary	96.00%
IVAM Regress	92.23%
PBL-McRBFN Binary (Babu and Suresh, 2013)	76.77%
PCA-SVM Binary (Scholkopf and Smola, 2002)	66.98%
IPCA-SVM Binary (Scholkopf and Smola, 2002)	69.70%
ICA-SVM Binary (Babu and Suresh, 2013)	62.80

IVAM Regressor was evaluated using 10-fold cross-validation with a mean-loss error. IVAM Binary was also evaluated using 10-fold cross validation, but using binary accuracy as the metric. The testing for the presence of Alzheimer's with the IVAM Binary yields a near perfect prediction rate which suggests that IVAM's source of error when running discrete classification comes from classifying between CDRs of 0.5 and 1.0.

References

Ashburner, J. and Friston, K. J. (2000). Voxel-based morphometry- the methods. *Neuroimage*, 11:805–821.

Babu, S. G. and Suresh, S. (2013). Meta-cognitive rbf network and its projection based learning algorithm for classification problems. *Cognitive Computation*, 6(2).

Bentley, J. L. (1975). Multidimensional binary search trees used for associative searching. *Commun. ACM*, 18(9):509–517.

Bianchetti, A., Ranieri, P., Margiotta, A., and Trabucchi, M. (2006). Pharmacological treatment of Alzheimer's Disease. *Aging clinical and experimental research*, 18(2)(158-162).

Buckner, R. L., Head, D., Parker, J., Fotenos, A. F., Marcus, D., Morris, J. C., and Snyder, A. Z. (2004). A unified approach for morphometric and functional data analysis in young, old, and demented adults using automated atlas-based head size normalization: reliability and validation against manual measurement of total intracranial volume. *Elsevier*, 23(2)(724-738).

Fennema-Notestine, C., Ozyurt, I. B., Clark, C. P., Morris, S., Bischoff-Grethe, A., Bondi, M. W., Jernigan, T. L., Fischl, B., Segonne, F., Shattuck, D. W., Leahy, R. M., Rex, D. E., Toga, A. W., Zou, K. H., and Brown, G. G. (2006). Quantitative evaluation of automated skull-stripping methods applied to contemporary and legacy images: effects of diagnosis, bias correction, and slice location. *Hum Brain Mapp*, 27(2):99–113.

Geurts, P., Ernst, D., and Wehenkel, L. (2006). Extremely randomized trees. *Machine Learning*, 63(1):3–42.

Kullback, S. and Leibler, R. A. (1951). On information and sufficiency. *Ann. Math. Statist.*, 22(1):79–86.

Mattes, D., David, H., Vessele, H., Lewellyn, T., and Eubank, W. (2001). Nonrigid multimodality image registration. *Medical Imaging*.

Murphy, K. P. (2012). *Machine learning: a probabilistic perspective*. Cambridge, MA.

Pedregosa, F., Varoquaux, G., Gramfort, A., Michel, V., Thirion, B., Grisel, O., Blondel, M., Prettenhofer, P., Weiss, R., Dubourg, V., Vanderplas, J., Passos, A., Cournapeau, D., Brucher, M., Perrot, M., and Duchesnay, E. (2011). Scikit-learn: Machine learning in Python. *Journal of Machine Learning Research*, 12:2825–2830.

Scholkopf, B. and Smola, A. J. (2002). Learning with kernels. *MIT Press*.

Speert, D., Benson, T., Cameron, J., Kaplan, B., Parfitt, D., and Roskams, A. J. (2012). *BrainFacts A Primer on the Brain and Nervous System*. Society for Neuroscience.

Veress, A. I., Klein, G., and Gullberg, G. T. (2013). A comparison of hyperelastic warping of pet images with tagged mri for the analysis of cardiac deformation. *Int. J. Biomedical Imaging*, 2013.

Ward, J. H. (1963). Hierarchical grouping to optimize an objective function. *Journal of the American Statistical Association*, 58(301):236–244.